ENSO Impact on Kelvin Waves and Associated Tropical Convection

GUI-YING YANG

National Centre for Atmospheric Science, and University of Reading, Reading, United Kingdom

BRIAN HOSKINS

University of Reading, Reading, and Grantham Institute for Climate Change, Imperial College London, London, United Kingdom

(Manuscript received 27 February 2013, in final form 2 May 2013)

ABSTRACT

The impact of El Niño–Southern Oscillation (ENSO) on atmospheric Kelvin waves and associated tropical convection is investigated using the ECMWF Re-Analysis, NOAA outgoing longwave radiation (OLR), and the analysis technique introduced in a previous study. It is found that the phase of ENSO has a substantial impact on Kelvin waves and associated convection over the equatorial central-eastern Pacific. El Niño (La Niña) events enhance (suppress) variability of the upper-tropospheric Kelvin wave and the associated convection there, in both extended boreal winter and summer.

The mechanism of the impact is through changes in the ENSO-related thermal conditions and the ambient flow. In El Niño years, because of SST increase in the equatorial central-eastern Pacific, variability of eastward-moving convection, which is mainly associated with Kelvin waves, intensifies in the region. In addition, owing to the weakening of the equatorial eastern Pacific westerly duct in the upper troposphere in El Niño years, Kelvin waves amplify there. In La Niña years, the opposite occurs. However, the stronger westerly duct in La Niña winters allows more NH extratropical Rossby wave activity to propagate equatorward and force Kelvin waves around 200 hPa, partially offsetting the in situ weakening effect of the stronger westerlies on the waves. In general, in El Niño years Kelvin waves are more convectively and vertically coupled and propagate more upward into the lower stratosphere over the central-eastern Pacific.

The ENSO impact in other regions is not clear, although in winter over the eastern Indian and western Pacific Oceans Kelvin waves and their associated convection are slightly weaker in El Niño than in La Niña years.

1. Introduction

The El Niño–Southern Oscillation (ENSO) is an intrinsic atmosphere–ocean coupled phenomenon in the tropical Pacific. Although ENSO originates in the tropical Pacific, it has a large impact on global climate and regional weather through various mechanisms, such as low-frequency teleconnections, ENSO-related tropical forcing, and ambient flows (e.g., Wallace and Gutzler 1981; Barnston and Livezey 1987; Kushnir and Wallace 1989; Zhang et al. 1996; Wang et al. 2000; Kawamura et al. 2001; Trenberth et al. 2002; Chou et al. 2003; Sakai and Kawamura 2009).

ENSO theories emphasize the role of wave dynamics on the initiation of ENSO, which involves both oceanic and atmospheric Kelvin waves and equatorial Rossby waves. On the other hand, ENSO-related changes in the ambient flow and thermal forcing would have an impact on equatorial waves in the atmosphere since a number of observational studies have shown that the zonal flow and convective forcing significantly affect their behavior (e.g., Yang et al. 2007a, 2011, 2012). A modeling study of Maury et al. (2013) found that the ENSO signal has a substantial influence on stratospheric equatorial Kelvin waves. However, there have been few observational studies of the ENSO impact on equatorial waves in the atmosphere, and there is very limited understanding of this.

Equatorial waves and tropical convection and their coupled behavior are fundamental components of the tropical climate system. A substantial fraction of the large-scale variability in convection at time scales less

Corresponding author address: Gui-Ying Yang, Department of Meteorology, University of Reading, Earley Gate, Reading RG6 6BB, United Kingdom.
E-mail: g.y.yang@reading.ac.uk

DOI: 10.1175/JAS-D-13-081.1

than 30 days is associated with equatorial waves (e.g., Redelsperger et al. 1998). Equatorial waves have been used to explain some fundamental phenomena of the tropical climate, such as the Walker circulation (e.g., Gill 1980), atmospheric teleconnection patterns (e.g., Lim and Chang 1983), the Madden–Julian oscillation (e.g., Lau and Peng 1987), as well as the forcing of the equatorial quasi-biennial oscillation (QBO) and semiannual oscillation in the stratosphere (e.g., Lindzen and Holton 1968). Because of ENSO's large impacts on global climate and regional weather activities, understanding the ENSO impact on equatorial waves is important for improvement of weather forecasting in the tropics and the extratropics on time scales beyond a few days and is also crucial for climate prediction (e.g., Lin et al. 2006; Ringer et al. 2006; Yang et al. 2009).

Most previous studies identify equatorial wave modes using filters in the zonal wavenumber–frequency domain related to the theoretical dispersion relationship with various equivalent depths. However, in the real atmosphere the complicated space–time dependence of the ambient state, the feedback from convective heating organized by the wave, nonlinearities, and nonuniform damping can all be expected to lead to distortion of the theoretical dispersion curves, at the very least. More fundamentally they may lead to the invalidity of the modal separation in the vertical, and hence the concept of equivalent depth. Consequently, different equatorial modes may not, in reality, be well separated in the frequency and zonal wavenumber domain. Also, it is unclear how much of the shallow-water theory of equatorial waves can be carried over to the real world.

A less constraining methodology for identifying equatorial waves, which does not assume that the linear adiabatic theory for equatorial waves on a resting atmosphere is directly applicable, was developed in Yang et al. (2003) (hereafter YHS) and has been applied to European Centre for Medium-Range Weather Forecasts (ECMWF) analysis data to investigate convectively coupled equatorial waves in the troposphere (Yang et al. 2007a,b,c; hereafter YHS07a,b,c) and the behavior of the equatorial waves under opposite phases of the QBO in the lower stratosphere (Yang et al. 2011, hereafter YHS11; Yang et al. 2012, hereafter YHG12), and has proved useful in the evaluation of the ability of model performance in the simulation of convectively coupled equatorial waves (Yang et al. 2009).

The aim of this study is to use YHS methodology and the Interim ECMWF Re-Analysis (ERA-Interim) datasets to investigate ENSO impact on Kelvin waves for both extended boreal winter (November–April) and summer (May–October) in the period from 1979 to 2010.

The outline of this paper is organized as follows. Section 2 describes the data and methodology. Section 3 describes the selection of El Niño and La Niña seasons. The overall variability of tropical convection is presented in section 4. The ENSO-related zonal flow, the variability of Kelvin waves, and their relationship are shown in section 5. Section 6 presents evidence of extratropical forcing of the Kelvin waves. The behavior of convectively coupled Kelvin waves is presented in section 7. Some conclusions and a discussion are given in section 8.

2. Data and methodology

The datasets used in this study are the ERA-Interim data, NOAA interpolated daily outgoing longwave radiation (OLR) for the period from 1979 to 2010, the Hadley Centre Sea Ice and Sea Surface Temperature data (HadISST), and the Southern Oscillation index provided by the Australian government Bureau of Meteorology archives. ERA-Interim is the latest global atmospheric reanalysis produced by the ECMWF. Multilevel ERA-Interim 6-hourly data are stored with a horizontal resolution of about 0.7° and at 37 pressure levels from 1000 to 1 hPa. Detailed information of the ERA-Interim data can be found in Dee et al. (2011) and OLR data in Liebmann and Smith (1996). The dynamical fields used to analyze equatorial waves are 6-hourly horizontal winds (u, v) and geopotential height (Z).

The methodology to identify equatorial waves developed in YHS is used to obtain various equatorial wave modes. The methodology does not assume that the linear adiabatic theory for equatorial waves on a resting atmosphere is directly applicable; in particular, the vertical structures and dispersion relations of theoretical equatorial waves are not imposed. As described in YHS and YHS07a, potential equatorial waves are identified by projecting the dynamical fields at each pressure level onto the horizontal structures given by equatorial wave theory.

Before projection, the dynamical fields are first separated into eastward- and westward-moving components using a space–time spectral analysis to filter the data in a domain of zonal wavenumber k from ± 2 to ± 10 and period from 2 to 30 days, which contains most equatorial waves. This filter includes a broader spatial–temporal domain than that which fits the usual shallow water dispersion curves. The eastward-moving component is used for the analysis of Kelvin waves.

The parabolic cylinder functions that describe the horizontal structures of theoretical equatorial waves were used as basis functions for projecting the horizontal winds and geopotential height into different wave modes, and this was done independently at a number of

pressure levels. The parabolic cylinder functions (D) take the form

$$D_r(y/y) = \exp[-(y/2y_0)^2]P_r(y/y_0),$$

where P_r is a polynomial of degree r and y_0 is the latitudinal trapping scale.

Meridional wind v is projected directly onto the parabolic cylinder functions and, as in Gill (1980), the variables $q = \alpha Z + u$ and $r = \alpha Z - u$ are also projected independently onto the different modes. Here α is determined from the trapping scale y_0, which is predetermined by a best fit of the v, q, and r fields in the latitude belt 20°N–20°S, as discussed in detail in YHS and YHG12 where a similar best-fit $y_0 = 6°$ was found. Therefore, in this study y_0 is chosen to be 6°.

Guided by basic equatorial wave theory and observational analyses, the parabolic cylinder function series expansions are organized and described as follows:

$$\begin{aligned} q &= q_0D_0 + q_1D_1 + \sum_{n=1}^{n=\infty} q_{n+1}D_{n+1} \\ v &= \quad 0 \quad + v_0D_0 + \sum_{n=1}^{n=\infty} v_nD_n \\ r &= \quad 0 \quad + \quad 0 \quad + \sum_{n=1}^{n=\infty} r_{n-1}D_{n-1} \\ &\quad\ \uparrow \qquad \uparrow \qquad \uparrow \\ &\quad n=-1 \quad n=0 \quad n=1,2\ldots . \end{aligned}$$

For our projection of the data at each level we will consider the $n = -1$ field (q_0) and refer to the eastward component as the Kelvin wave. Together the $n = 0$ fields (q_1 and v_0) will be considered to describe the mixed Rossby gravity (MRG) wave, with the eastward component referred to as EMRG and the westward component referred to as WMRG. In theory, the $n = 1$ fields (q_2, v_1, r_0) describe three waves: the westward-moving Rossby wave, R1, and the eastward- and westward-moving gravity waves. High-frequency gravity waves are found to be weak so that the westward $n = 1$ structure is considered to represent the R1 wave.

In basic equatorial wave theory, the trapping scale y_0 is related to the gravity wave speed (c) and the equivalent depth (h) by $y_0 = (c/2\beta)^{1/2} = (gh)^{1/4}/(2\beta)^{1/2}$; thus, $h \sim y_0^4$ and $c \sim y_0^2$. The powers of y_0 in these expressions indicate that the vertical structure, which is dependent on h, and the phase speed c are likely to be much more sensitive than the horizontal structure functions, which are dependent on y_0. It is these structure functions that are used as the basis for our analysis. We allow these properties to emerge from the data. However, in equatorial wave theory, α is taken to be equal to $gc^{-1} \sim y_0^{-2}$, so there could be some sensitivity in the current analysis technique in the separation of u and Z into q and r. Nevertheless, YHS and YHG12 indicate that analysis using different values for y_0 shows that the structures and phase speed of equatorial waves are not in fact sensitive to the choice of y_0.

Linear regression techniques similar to YHS07a,b are used in sections 6 and 7 to examine extratropical forcing and composite horizontal/vertical structures of convectively coupled Kelvin waves and the spatial/temporal relationships between convection and waves. The regressions are based on considering the second field (the dependent variable) as a function of space and time in terms of its longitudinal relationship to extrema in the first field (the independent variable) that exceeds a threshold. As such it has some similarity with the centered composite analysis technique of Weare (2006). Details of the technique are described in YHS07a,b.

Owing to the large seasonal variability of equatorial waves, for the analysis here the year is split into two 6-month periods: an extended boreal winter (November–April) and summer (May–October), hereafter referred to as ''winter'' and ''summer.''

3. Selection of El Niño and La Niña seasons

Although there are a number of ways to define an El Niño or La Niña event, perhaps the most usual way is to use the Niño-3.4 index and Southern Oscillation index (SOI). The Niño-3.4 index is based on the averaged sea surface temperature anomaly (SSTA) in 5°S–5°N, 120°–170°W, a region with large variability on ENSO time scales. The SOI used here is the standardized anomaly of the monthly mean sea level pressure difference between Tahiti and Darwin, divided by the standard deviation of the difference and multiplied by 10 (Troup 1965). Using this method, the SOI ranges from about −35 to +35 with negative (positive) values associated with El Niño (La Niña) conditions.

Figure 1 shows seasonal mean Niño-3.4 SSTA and SOI anomalies (SOIA) in winter and summer, with respect to the seasonal cycle over 32 years from 1979 to 2010. An El Niño (La Niña) season is identified if the 6-month mean SSTA is equal to or exceeds +0.5°C (−0.5°C) with at least four consecutive months exceeding +0.4°C (−0.4°C), and the absolute value of seasonal mean of SOIA > 4 (< -4).

The thresholds for the SSTA and SOIA are indicated by pairs of solid and dotted lines, respectively. There are seven El Niño winters (1982/83, 1986/87, 1991/92, 1994/95, 1997/98, 2002/03, and 2009/10), seven La Niña winters (1988/89, 1998/99, 1999/00, 2000/01, 2005/06, 2007/08, and 2008/09), five El Niño summers (1982, 1987, 1991,

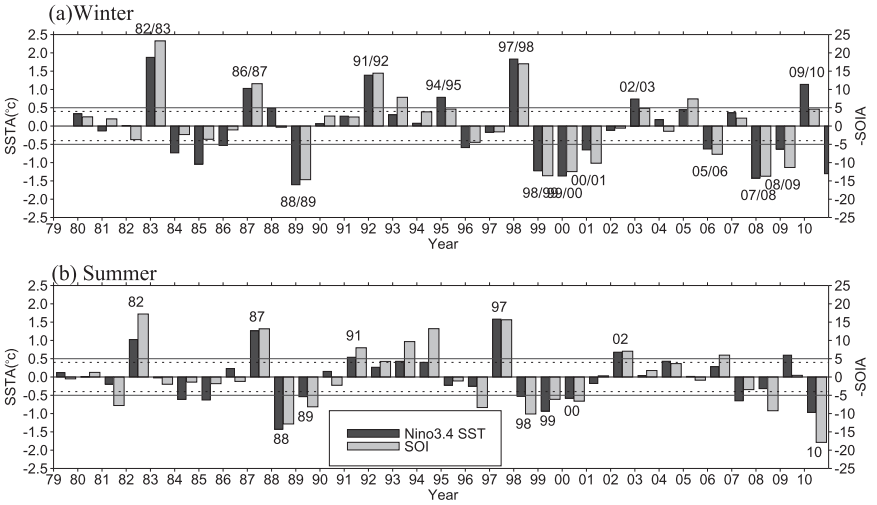

FIG. 1. Seasonal means of Niño-3.4 SST anomalies (SSTA, °C) and Southern Oscillation index anomaly (SOIA) for 1979–2010 in (a) winter (November–April) and (b) summer (May–October). Note that the SOIA is reversed in sign so as to be in line with SST. The two solid lines indicate the threshold SSTA of ±0.5°C and the two dotted lines indicate the threshold SOIA of ±4, used to define El Niño and La Niña seasons. The numbers indicate the El Niño and La Niña seasons defined for winter and summer.

1997, and 2002), and six La Niña summers (1988, 1989, 1998, 1999, 2000, and 2010). These seasons are indicated by the dates associated with them in Fig. 1. It is noted that there are some nonselected seasons (consecutive seasons during 1983–86, winter 1995/96, and summer 2009) that have SSTA exceeding 0.5°C but SOIA being less than 4, and some other seasons (summer 1981, 1993, 1994, 1996, 2006, and 2008; winter 1992/93 and 2004/05) with SOIA exceeding 4 but SSTA less than 0.5°C .

For a more detailed view of ENSO evolution in the period covered by the data a Hovmöller plot of monthly equatorial SSTA is given in the appendix (Fig. A1a), where these El Niño and La Niña seasons are indicated. Also shown are the equatorial OLR and its standard deviations.

4. Tropical convective variability

a. Power spectra

Spatial–time power spectral analysis is performed to investigate the convective variability associated with equatorial waves. Since tropical convection is different in the two longitudinal hemispheres, the power spectra are calculated separately for the Eastern Hemisphere (EH) and Western Hemisphere (WH). To focus on the Kelvin wave–related convection, Fig. 2 shows OLR power spectra of the symmetric component composite/averaged for El Niño and La Niña seasons. The power is averaged over 15°N–15°S and divided by the background power. In all cases, spectral peaks in the eastward-moving component are generally consistent with the theoretical dispersion curves of Kelvin waves for various equivalent depths. Another peak in the lower frequency band is also evident, which is associated with the eastward-moving Madden–Julian oscillation. Although dispersion curves of $n = 1$ Rossby (R1) waves are also shown in the westward-moving component, the R1 waves will be discussed in a subsequent paper.

It is clear that the Kelvin wave–related convection varies with ENSO phases and with hemispheres, both for winter and summer. In La Niña years, Kelvin wave–related convective signal is stronger in the EH than in the WH, as in the case for the climatological mean state with convection being stronger over the EH warm water region. However, in El Niño years, the Kelvin wave–related convective signal is stronger in the WH than in the EH. The ENSO-related difference is more obvious in the WH, with the Kelvin wave–related power being much stronger in El Niño than in La Niña. In the EH, the power shows an opposite tendency to that in the WH but the ENSO-related difference is smaller. Owing to the dominant difference in the WH, power spectra obtained from the whole (global) tropical domain still indicate a stronger signal in the El Niño year than the La Niña year. This contrasts with Wheeler and Kiladis (1999), who indicated that the appearance of the OLR spectra is not significantly modified by ENSO phases.

The different power intensity exhibited in the composite field is also present in each case, with the Kelvin wave signal being stronger in El Niño than in La Niña

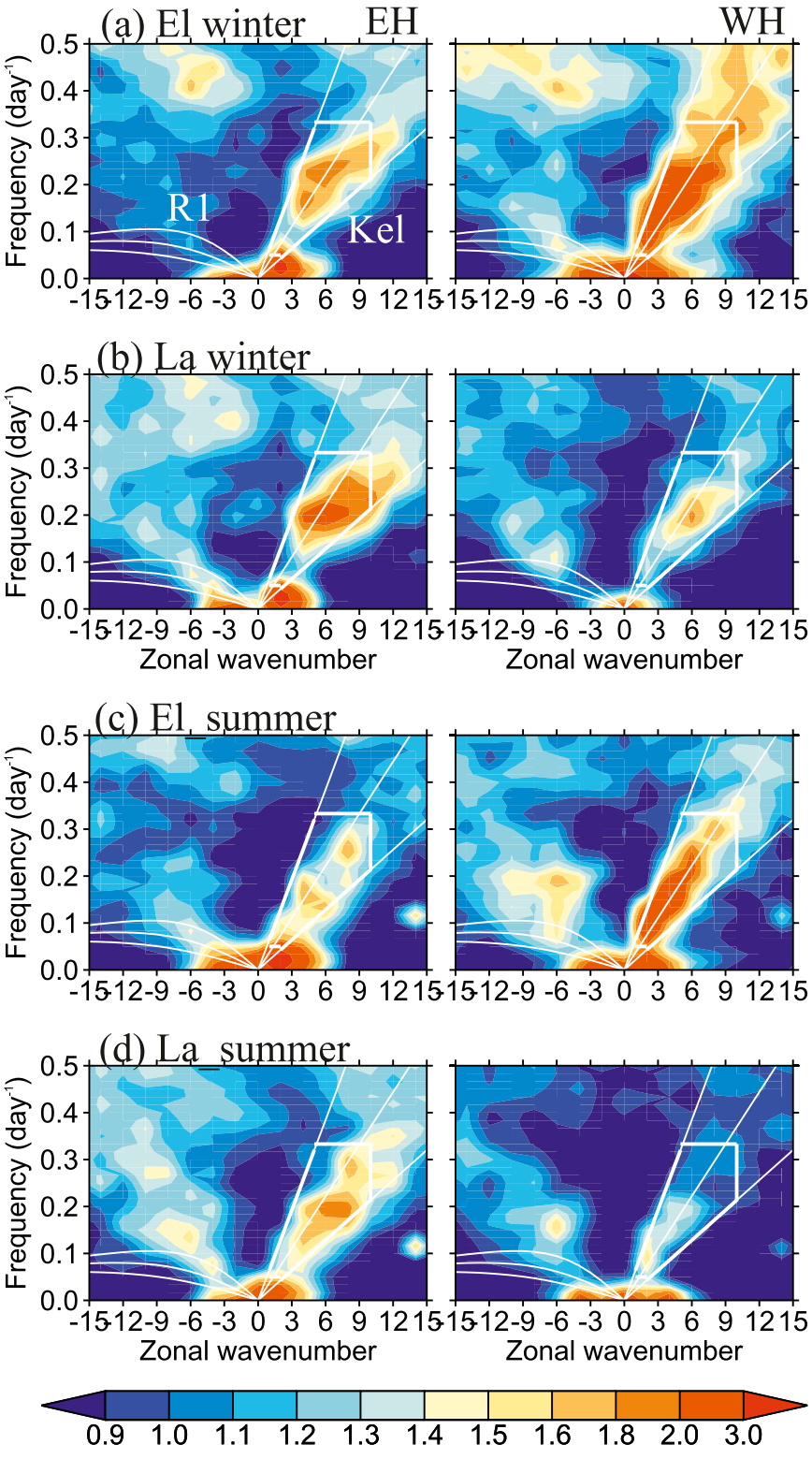

FIG. 2. El Niño and La Niña composites of zonal wavenumber–frequency power spectra of the symmetric components of tropical OLR in the (left) EH and (right) WH, averaged over 15°N–15°S and divided by the background power for (a),(b) winter and (c),(d) summer. Superimposed lines are the dispersion curves for Kelvin and R1 waves, with equivalent depths 10, 30, and 90 m. Thick lines indicate the Kelvin wave domain used for filtering OLR in Fig. 3.

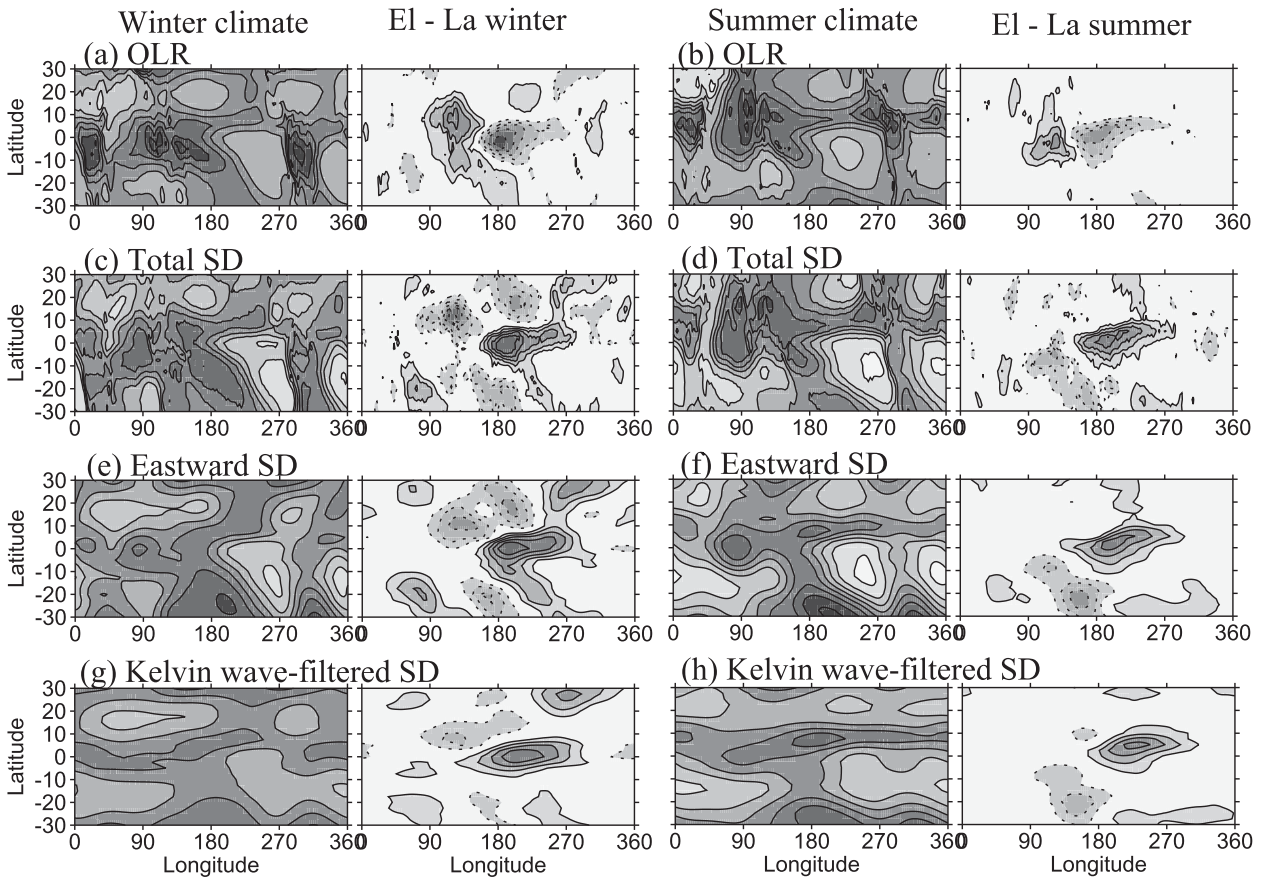

FIG. 3. Seasonal climatological means and differences ($W m^{-2}$) between El Niño and La Niña for (a),(b) OLR, (c),(d) OLR standard deviation (SD), (e),(f) eastward-moving OLR SD, and (g),(h) Kelvin wave–filtered OLR SD, for (left two columns) winter and (right two columns) summer. Contours are for positive (solid) and negative (dotted) values, and the zero contour is not drawn. The contour interval is, respectively, 15 and 10 for OLR and its difference, 6 and 4 for total OLR SD and its difference, 1.2 and 0.8 for eastward OLR SD and its difference, and 1.0 and 0.6 for Kelvin wave–filtered SD and its difference.

(not shown). This indicates that the difference of Kelvin wave–related convection between ENSO phases is robust.

In addition to the difference in the power intensity, Fig. 2 also shows some difference in the frequencies/phase speeds of the convective signal. The convective signal seems to appear at higher frequency (or higher equivalent depths and faster phase speeds) in El Niño winter than in La Niña winter.

b. Geographic distribution

To examine the geographic distribution of tropical convection and its general variability in different seasons, the climatological seasonal-mean OLR and its total standard deviation (daily data departure from monthly mean) are shown in Figs. 3a–d. To show the fraction of the large-scale variability associated with transient propagating convection, the standard deviations of eastward-moving OLR and Kelvin wave–filtered OLR are given in Figs. 3e–h. The eastward-moving OLR is filtered in a zonal wavenumber–frequency domain with k from 2 to 10 and period from 3 to 30 days, which contains large-scale submonthly variability. The Kelvin wave–related OLR is filtered using the dispersion relation domain shown in Fig. 2, the domain being within but smaller than that of the eastward-moving domain. The climatological seasonal means are shown in the first and third columns, and the differences between the two ENSO phases are shown in the second and fourth columns for winter and summer, respectively.

Figures 3a–d show that tropical convection is generally stronger in the EH than in the WH. The areas of larger total standard deviation (SD) are coincident with the areas of stronger convection, indicated by the lower mean values of OLR, in agreement with other observational and modeling studies (e.g., Salby et al. 1991; Slingo et al. 1992). The monthly evolution of equatorial convection and its standard deviation are given in the appendix (Figs. A1b,c), where it is shown that the OLR

SD anomalies have a significant ENSO-related signal over the equatorial central-eastern Pacific, with positive SD anomalies coincident with regions of negative OLR anomalies and warm SST there, and vice versa for negative SD anomalies.

Figures 3e,f show that the eastward-moving OLR SD accounts about one-quarter of the total SD in the tropics (20°N–20°S) and one-third in the subtropics. The Kelvin wave–related SD accounts for about two-thirds of the eastward-moving SD and about 16% of the total SD in the tropics. This indicates that a substantial fraction of the large-scale variability in eastward-moving convection at time scales less than 30 days is associated with Kelvin waves. All types of variability are mainly centered on the equator over the EH warm water region, but to the north of the equator over the Pacific ITCZ region, except that in summer the total variability also has a large amplitude over the Asian summer monsoon region.

In the difference fields (El Niño minus La Niña), all types of variability show positive SD in the equatorial central-eastern Pacific where the convective signal is normally weak in the climatological mean. The positive SD area is also coincident with the negative OLR anomalies there. It is seen that the positive total SD and negative OLR are more centered over the central Pacific, whereas the eastward-moving and Kelvin wave–filtered positive SD tend to spread slightly eastward to the eastern Pacific. This is consistent with the power spectral result in Fig. 2, which shows that the WH Kelvin wave–filtered convective signal is stronger in El Niño than in La Niña years.

Consistent with the main convective region shifting eastward to the central Pacific, the difference fields show that in winter there is positive OLR over the tropical western Pacific (90°–160°E) with a peak at 10°N, 120°E, in agreement with Wang et al. (2000) that precipitation around the Philippine Sea has a negative anomaly in El Niño years. The positive OLR extends southeast to the central South Pacific, accompanied by negative SD there but the SD signal is very weak around the equator. There is also negative SD in the central-eastern North Pacific (15°–30°N, 160°E–150°W) region, accompanied by positive OLR there. As will be shown in section 6, this may be associated with weaker NH extratropical forcing in the central-eastern Pacific in El Niño winters than in La Niña winters. These features and other details are all very similar to that shown in Matthews and Kiladis (1999) for the December–February (DJF) difference between strong and weak NH subtropical jets, which roughly correspond to warm and cold ENSO phases (see their Figs. 3c and 5c).

In summer the ENSO-related difference pattern is relatively simple, dominated by a pattern of negative OLR and positive SD over the central-eastern Pacific, as in the winter case. It is also seen that the ENSO-related difference is weaker than that in winter, consistent with the observation that ENSO has strong ''phase locking'' to the seasonal cycle, the peak phases of El Niño and La Niña tending to occur around boreal winter (Rasmusson and Carpenter 1982).

It is noted that for both winter and summer, there is positive OLR over the equatorial western Pacific (90°–150°E), consistent with the convection in the western Pacific being intensified in La Niña years. However, there is no corresponding negative SD for all types of variability near the equator. This is because, in La Niña years, convection over the equatorial western Pacific does not have much variability on time scales shorter than one month, as indicated in the appendix (Fig. A1c). The exceptions to this are the two strongest El Niño events (1982–83 and 1997–98), which are accompanied by abnormally weak submonthly variability over the western Pacific (Fig. A1c). Further analysis indicates that even these SDs filtered in a lower-frequency band (period 30–90 days) do not show much ENSO-related difference around the equatorial western Pacific. This is suggestive that the ENSO-related convective variability there has time scales longer than a season.

To examine if the differences in the composite fields also appear in each ENSO event, Fig. 4 gives the zonal distribution of equatorial eastward-moving and Kelvin wave–filtered OLR variability in each El Niño and La Niña season. For comparison, the equatorial SST is also given in the top panel. It is apparent that the warm (cold) equatorial SST in the central-eastern Pacific region appears for each El Niño (La Niña) year. A remarkable difference between ENSO phases is consistently found over the central-eastern Pacific for both eastward-moving and Kevin wave–filtered OLR variability. In La Niña winters, the two types of OLR variability are consistently stronger in the Indian–western Pacific than in the central-eastern Pacific, similar to the normal conditions but with a stronger tendency. However, in El Niño winters, convective variability is clearly increased over the central-eastern Pacific, consistent with warmer SST there. There is a clear connection between the amount of SST warming and the intensity of eastward-moving and Kevin wave–filtered OLR SD. For the three strongest El Niño winters— 1982/83, 1991/92, and 1997/98—the convective signals there are even stronger than their counterpart over the Indian–western Pacific Ocean. For other El Niño events that do not have the full eastern Pacific warming, the increase in their convective activity is less.

The equatorial Kelvin wave–filtered SD accounts for about 70% of the eastward SD and there is a very

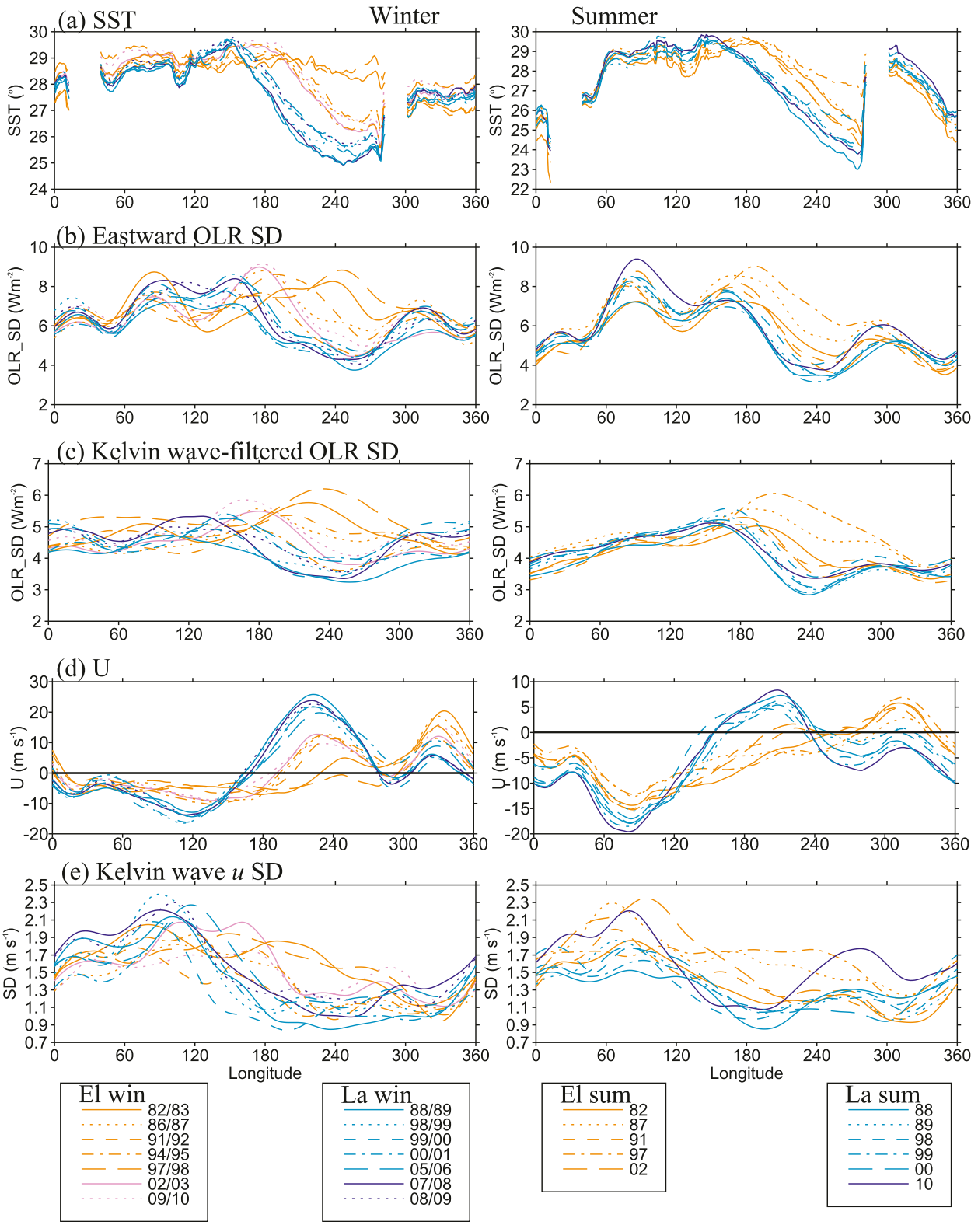

FIG. 4. Longitudinal distribution of (a) SST at 7.5°N–7.5°S, (b) eastward-moving OLR SD at 10°N–10°S, (c) Kelvin wave–filtered OLR SD at 10°N–10°S, (d) 100–200-hPa ambient zonal winds at 5°N–5°S, and (e) Kelvin wave equatorial *u* SD at 100–125 hPa, for each El Niño and La Niña (left) winter and (right) summer.

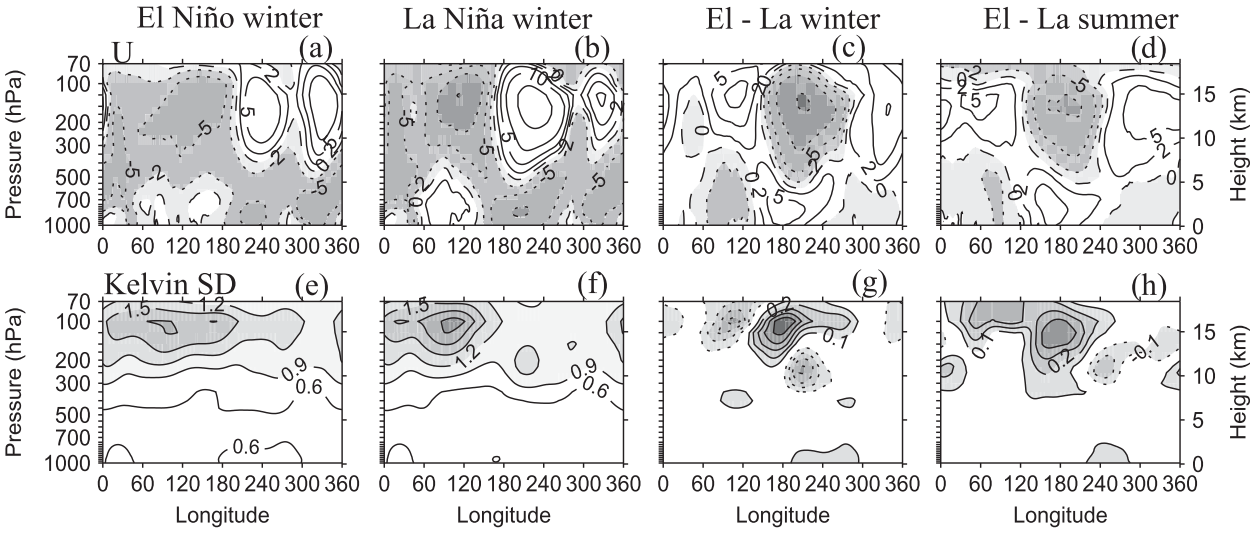

FIG. 5. Longitude–height section of El Niño and La Niña composites and the difference between them for (a) equatorial (5°N–5°S) ambient zonal winds U ($m\,s^{-1}$) and (b) Kelvin wave equatorial u SD ($m\,s^{-1}$) for (left) El Niño winters, (second column) La Niña winters, (third column) the difference between El Niño and La Niña winters, and (right) the difference between El Niño and La Niña summers.

consistent relationship between them over the central-eastern Pacific, indicating that the eastward-moving variability is dominated by the Kelvin wave–filtered variability in the region. In contrast, the consistency is less clear in the winter EH. For example, the Kelvin wave–filtered SD is stronger over Indian Ocean (40°–100°E) for the three strongest El Niño winters, consistent with the warmest SST there, but the feature is less clear for the eastward-moving SD. On the other hand, in El Niño winters the eastward-moving SD is consistently weaker over the Maritime Continent–western Pacific region (110°–140°E), but this is not clear for Kelvin wave–filtered SD.

In summer, both eastward-moving and Kelvin wave–filtered variability over the central-eastern Pacific are also consistently stronger in each El Niño than in each La Niña, with the strongest amplitude there occurring in the three strongest El Niño summers—1982, 1987, and 1997—consistent with the warmest SST being there. An obvious difference between the two types of variability in the EH is that, unlike the eastward-moving SD, the Kelvin wave–filtered SD does not show a peak over the Indian Ocean.

Figures 4d,e also give the equatorial zonal flow and variability of Kelvin wave equatorial u for comparison with the convective variability. They will be discussed in the next section.

5. Ambient zonal flow and variability of Kelvin wave winds

A number of studies show that equatorial wave activity exhibits zonal and vertical variations that are partly due to variations of the ambient zonal flow (e.g., YHS07a; YHS11; YHG12). To examine the overall variability of Kelvin waves in different ENSO phases and its relationship with the ENSO-related variation in the zonal flow, Fig. 5 shows longitude–height sections of equatorial zonal flow (U) and standard deviations of Kelvin wave winds composite in El Niño and La Niña winters, and the difference between the two ENSO phases in both winter and summer. Kelvin wave activity is measured by the equatorial u. Note that, because the latitudinal structures are specified, the pictures for the Kevin wave are independent of the latitude chosen and only the contour interval would change.

Figures 5a,b show that in the winter upper troposphere there are easterly winds prevalent in the EH and westerly winds prevalent in the WH. In the lower troposphere zonal winds are weaker and generally have reversed sign with those in the upper troposphere. In El Niño winters, owing to the main convective region moving eastward, the upper-level divergence and lower-level convergence in the zonal winds move eastward, and hence the EH upper-tropospheric easterlies and lower-tropospheric westerlies are both weakened and move eastward. Because of the upper-tropospheric easterlies extending past the date line, the upper-tropospheric ''westerly duct'' over the equatorial eastern Pacific is clearly weakened but the westerly duct over the Atlantic is intensified. The contrast of the zonal flow between ENSO phases is clearly shown in the difference field (Fig. 5c). It is seen that the two westerly ducts differ significantly between ENSO phases, with the eastern

Pacific duct being much weaker in El Niño winters than in La Niña winters and vice versa for the Atlantic duct. In summer, the two westerly ducts are much weaker, with the eastern Pacific duct only appearing in La Niña conditions and the Atlantic duct appearing in El Niño conditions (not shown here but seen in Fig. 4d). The difference is shown in Fig. 5d.

Figures 5e,f show that the Kelvin wave winds have the greatest amplitude around 125–100 hPa over the warm waters of the EH with a peak centered on 90°E in winter (60°E in summer, not shown). The large amplitude of the Kelvin wave in the EH coincides with the easterly flow in the upper troposphere. This can be explained by the notion that the wave action density ξ is conserved following a ray (e.g., Bretherton and Garrett 1968). Here $\xi = E/\omega_i$, where E is the energy density of the wave and ω_i is the intrinsic frequency of the wave. For the Kelvin wave ($\omega_i > 0$ and constant along a ray) its energy $E = \xi\omega_i = \xi(\omega - Uk)$ is large in ambient easterly winds and increases with wind strength, but small in westerly winds and decreases with wind strength. The relationship is also indicated in the modeling studies of Wang and Xie (1996) and Hoskins and Yang (2000). They show that Kelvin waves are stronger in an easterly wind region and westward-moving waves are stronger in a westerly region.

It is clear that the Kelvin wave amplitude varies with ENSO phases and that the variation is consistent with the ENSO-induced change in the ambient flow. First, the Kelvin wave peak at 125–100 hPa over the eastern Indian Ocean–western Pacific is weaker in El Niño than La Niña winters, consistent with the reduced easterly flow in El Niño winters. Second, in El Niño winters the area of large Kelvin wave amplitude at 125–100 hPa extends farther eastward into the central-eastern Pacific and intensifies the wave there, whereas in La Niña winters it is more confined to the west of the date line. This is also consistent with the fact that the upper-tropospheric westerly flow, especially the Pacific westerly duct, is weaker in El Niño than in La Niña. The relationship is further shown in the difference field, where a large area of positive wave amplitude is coincident with the upper-tropospheric easterly anomaly in the central-eastern Pacific and an area of negative amplitude is coincident with the westerly anomaly over the eastern Indian–western Pacific Oceans.

However, in La Niña winters there is also a localized peak at 200 hPa, 150°W embedded in the stronger Pacific westerly duct (Fig. 5f). Analysis of an individual event indicates that the local maximum exists in almost all La Niña winters, with the standard deviation value at 200 hPa, 150°W ranging between 1.2 and 1.5, consistently larger than for El Niño winters that have values in the range of 0.8–10. The only exception is the strongest 1997/98 El Niño winter that has a value of 1.3, which is likely due to the strong thermal forcing in the entire central-eastern Pacific. Therefore, in the difference field there is a negative wave amplitude area appearing in the region of the easterly anomaly (Fig. 5g). As will be shown in the next section, this is associated with the NH extratropical forcing there.

In summer, owing to the Pacific duct and associated extratropical forcing being weak, the Kelvin wave tends to be influenced only by the in situ zonal flow, and the difference is consistent with this, there being a larger area of positive amplitude coincident with the easterly anomaly (Fig. 5h). However, the amplitude of the difference is weaker than that in winter (Fig. 5g). In contrast to the winter case, the ENSO-related Kelvin wave difference also shows a positive sign above 125 hPa over the Indian–western Pacific Oceans. This is consistent with the easterly anomaly above 100 hPa but not with the westerly flow below that level.

The zonal flow and Kelvin wave amplitude in each El Niño and La Niña season have been shown in Figs. 4d,e for comparison with the convection there. It is seen that the composite features shown in Fig. 5 also appear in each case. Over the central-eastern Pacific the zonal flows clearly differ between ENSO phases. The eastern Pacific westerly duct is consistently much weaker in El Niño than in La Niña winters, and the prevailing westerly becomes easterly for the 1997/98 El Niño winter. The summer Pacific westerly duct only exists in La Niña conditions. In five out of seven El Niño winters, the Kelvin wave amplitude over the central Pacific tends to be stronger, with the two strongest amplitudes in 1982/83 and 1997/98 being consistent with the weakest Pacific westerly duct. In summer, Kelvin wave variability over the central-eastern Pacific is also consistently stronger in El Niño than in La Niña except for the 2010 La Niña.

Although there is good consistency of the Kelvin wave amplitude and the ambient flow over the central-eastern Pacific, the stronger Kelvin wave amplitude in El Niño years is also consistent with the warmer SST and enhanced equatorial convective signal there (Figs. 4a–c). This is in agreement with YHS07a,b and YHS11 that the longitudinal variation of equatorial wave activity in the upper troposphere depends on the zonal flow and convective forcing.

It is also seen in Fig. 4e that in winter the Kelvin wave amplitude around 80°–120°E tends to be weaker in most El Niño winters, consistent with the weaker easterly flow (Fig. 4d) and weaker eastward-moving convection (Fig. 4b) there, but surprisingly it is not consistent with the Kelvin wave–filtered convection (Fig. 4c). It appears that convection filtered in a larger spectral domain of eastward-moving activity, as used in YHS07a,b, is better at capturing the coupling with Kelvin waves.

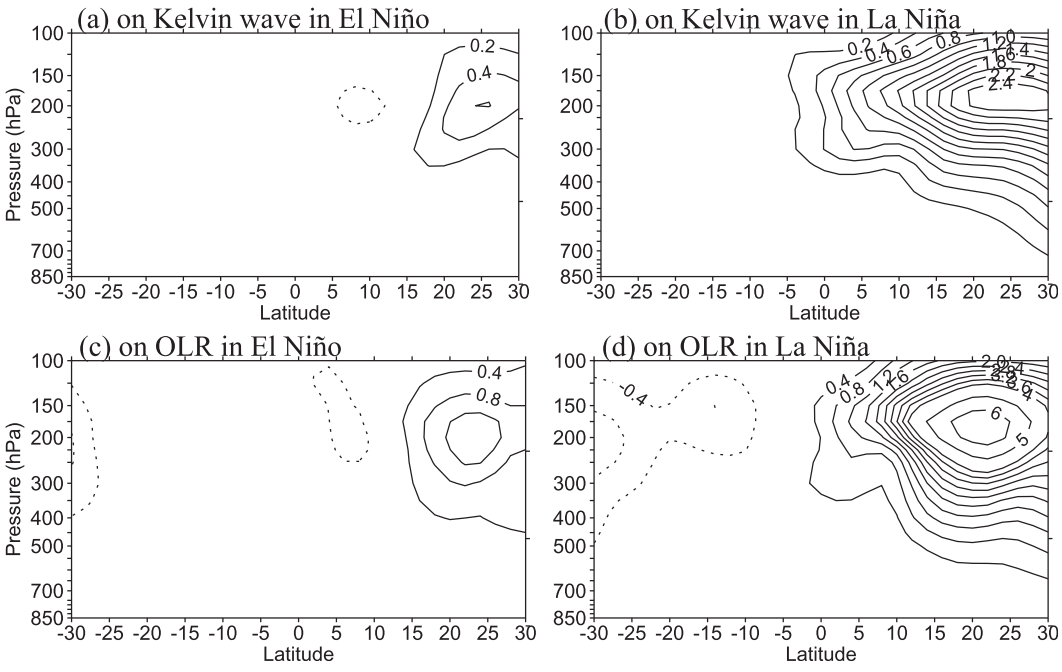

FIG. 6. Latitude–pressure sections of horizontal eddy momentum flux ($m^2 s^{-2}$) [u^*v^*] at 200 hPa regressed onto the extrema of (a),(b) 200-hPa Kelvin wave equatorial u and (c),(d) equatorial (10°N–10°S) eastward-moving OLR, in the eastern Pacific westerly duct region (180°–120°W) for (left) El Niño and (right) La Niña winter. The extrema of u and OLR have values 1.5 times the peak SD in the region; solid (dotted) lines are for positive (negative) values.

It is noticed that, although the Atlantic westerly duct is consistently stronger in El Niño than in La Niña years, the Kelvin waves over the region are not obviously weaker in El Niño. One reason for this could be that the ENSO-related difference in the Atlantic westerly duct is much smaller than that of the Pacific duct. However, a more important reason could be that the SST and convection there do not show ENSO-related differences. This is again in agreement with YHS07a,b that the Kelvin wave is more sensitive to the boundary thermal condition and more closely coupled with convection than other equatorial wave modes.

6. Extratropical forcing of the Kelvin wave

As mentioned above, a local maximum of Kelvin wave amplitude appears around 200 hPa, 150°W in La Niña winters (Fig. 5f). Since it occurs in the strong eastern Pacific westerly duct and Yang and Hoskins (1996) indicated that midlatitude nonstationary Rossby waves with eastward phase speeds can propagate into the equatorial region with reasonably strong westerly flow, therefore the stronger Kelvin wave amplitude there may be associated with an upper-tropospheric forcing of extratropical Rossby waves. To investigate wave meridional propagation, the horizontal eddy momentum flux [u^*v^*] associated with the 200-hPa Kelvin wave at 180°–120°W is shown in Figs. 6a,b. Here $u^* = u - [u]$ and $v^* = v - [v]$ are horizontal wind perturbations from mean winds [u] and [v] averaged over longitudinal displacements 60° to the west and east; u and v are eastward-moving winds that have been regressed onto the extrema in the Kelvin wave equatorial zonal wind. It is seen that in El Niño winters, [u^*v^*] is very weak and confined to the subtropical region, whereas in La Niña winters there is strong positive [u^*v^*] in the upper troposphere extending into the equatorial region. The strength of [u^*v^*] in neutral winters is between El Niño and La Niña winters (not shown). Since positive [u^*v^*] in the NH is indicative of Rossby wave activity propagating southward toward the tropics, this supports the suggestion that in La Niña winters when the eastern Pacific westerly duct is stronger there is more extratropical Rossby wave activity propagating into the equatorial region and this forces the 200-hPa Kelvin wave. Further analysis indicates that [u^*v^*] regressed onto Kelvin waves at other levels is generally much weaker than that found for 200 hPa. However, it is of interest that the strongest signal still appears at 200 hPa, even for regression on the Kelvin waves at 850 hPa. This strongly suggests that the extratropical forcing of the Kelvin wave is largest around 200 hPa.

A similar analysis has also been performed for the NH summer. Regression onto the 500-hPa Kelvin wave shows

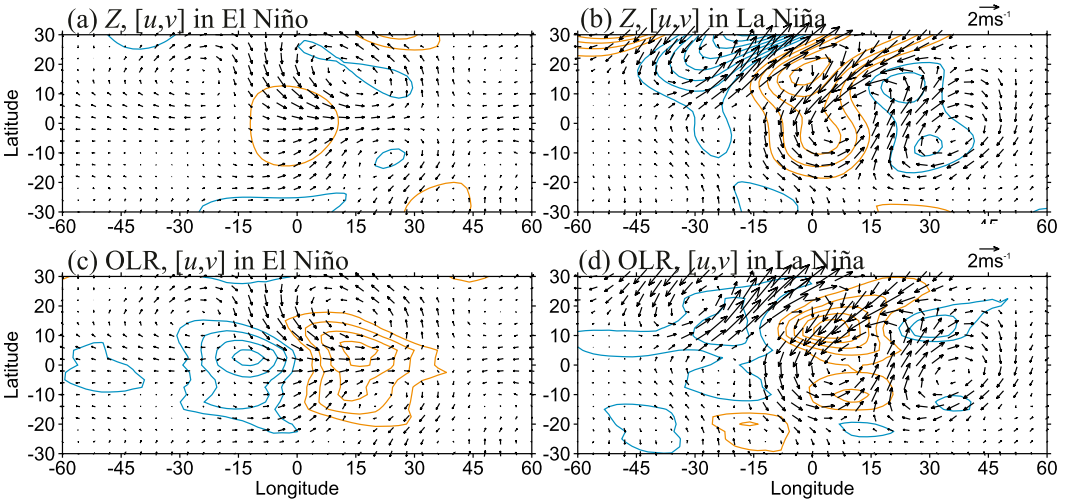

FIG. 7. 200-hPa eastward-moving horizontal winds (vectors) and (a),(b) geopotential height (Z), and (c),(d) OLR in (left) El Niño and (right) La Niña winters, regressed onto the extrema of Kelvin wave equatorial u for 180°–120°W. The extreme u is taken to be westerly and located at 0° relative longitude, with a positive value of 1.5 times its peak SD. The red (blue) contours are for positive (negative) Z or OLR, contour interval 2 m for Z and 1 W m^{-2} for OLR; the zero contour is not drawn.

the strongest signal of extratropical forcing, which again comes from the winter hemisphere but this time in the SH. However, in this season the signal extends less to the equatorial region and is very similar for two ENSO phases. It is noteworthy that in this season vertical velocity regressed onto the 500-hPa Kelvin wave exhibits a strong extratropical signal that extends fully into the equatorial region in the middle upper troposphere. This SH extratropical forcing of the Kelvin wave in summer was also found in YHS07c.

To examine the relationship of the extratropical forcing with tropical convection in winter, Figs. 6c,d also give the $[u^*v^*]$ regressed onto the extrema of OLR averaged at 10°N–10°S. A very similar pattern to Figs. 6a,b is seen in the NH. However, in La Niña winters the positive $[u^*v^*]$ extends less across the equator because there is also weak negative $[u^*v^*]$ in the SH, also indicative of equatorward propagation. This suggests that in La Niña winters the SH extratropical Rossby waves also have an impact on the tropical eastward-moving convection over the central-eastern Pacific.

To indicate the associated horizontal circulation, Fig. 7 gives the horizontal winds and geopotential height at 200 hPa for eastward-moving activity regressed onto the extrema of Kelvin wave equatorial u at 200 hPa, 180°–120°W. The extreme u is taken to be westerly and relocated at 0° relative longitude. In El Niño winters, the regressed fields are clearly dominated by a Kelvin wave structure with tropical u and Z being in phase and centered on the equator. In the NH subtropical region there is also a sign of a Rossby wave train but it is very weak. In contrast, in La Niña winters there is a very strong extratropical Rossby wave train with a northeast–southwest tilt, propagating into the equatorial region, consistent with the strong $[u^*v^*]$ shown in Fig. 6b. The strong positive Z around 0° longitude is consistent with the Kelvin wave structure. However, there is no clear westerly wind because of the coexistence of the Kelvin wave and an eastward-moving R1 wave that is also forced by the extratropical Rossby wave. The sign of the eastward-moving R1 wave can be seen with a pair of cyclones around 30° longitude and a pair of anticyclones around 0° longitude. Horizontal winds and geopotential height have also been regressed onto the eastward R1 wave (not shown). In El Niño winters, these fields look very different from those regressed onto the Kevin wave. In contrast, in La Niña winters, they are very similar to those regressed onto the Kelvin wave. This supports the hypothesis that in La Niña winters extratropical wave activity forces both Kelvin and R1 waves. The Kelvin and R1 waves have a certain phase relationship (perhaps consistent with their connection through convection, as shown in Fig. 6), such that the Kelvin wave westerly is in phase with the pair of anticyclone of the R1 wave around 0° longitude. This leads to their zonal winds having opposite signs but the Z fields having the same sign; therefore, the u field is weak but Z is very strong in the equatorial region. Owing to the interference of the two waves, the R1 wave looks less coherent because of the weakening of equatorial zonal winds.

Figures 7c,d show similar plots but the superimposed contours are the regressed eastward-moving OLR. In El Niño winters, the negative and positive OLR signals centered and symmetric about the equator are clearly in

phase with the divergence and convergence of the zonal winds, as expected for convectively couple Kelvin waves. However, in La Niña winters, there are pairs of positive and negative OLR that are off the equator and nearly symmetric about the equator but with an equatorial component. This further supports the coexistence of the Kelvin and R1 waves. The relationship between horizontal wind and convection in the NH (Fig. 7d) is consistent with that found in Kiladis (1998), who indicated that intensified convection appears in the region of the poleward flow ahead of upper-level troughs (cyclonic anomalies) in the wave train over the central Pacific. The NH off-equatorial convection in La Niña winters is consistent with that shown in Fig. 3, where the difference fields show positive OLR and negative OLR SD in the central North Pacific (15°–30°N, 160°E–130°W).

Although the NH extratropical forcing leads to a local Kelvin wave peak at 200 hPa in La Niña winters, which partly offsets the in situ weakening effect of the stronger ambient westerly wind on the waves, it is found that the waves are less vertically coupled. The correlation of the wave at 200 hPa with the wave at 850 hPa is −0.37, weaker than that in El Niño winters (−0.54). Its correlation with the wave at 100 hPa is also slightly weaker in La Niña winters. A few factors may contribute to the weaker vertical coupling: the extratropical forcing being only evident in the upper troposphere; the Kelvin wave interfering with the R1 wave; and weak convective coupling due to weaker equatorial convection in La Niña conditions.

It should be pointed out that the reduction in extratropical Rossby waves propagating into the equatorial region in El Niño winters is not only caused by the weaker westerly duct over the eastern Pacific. Another reason is that in El Niño winters the NH subtropical jet is strengthened over the Pacific and acts as a stronger and more continuous waveguide for extratropical Rossby waves, reducing their equatorward propagation into the eastern Pacific westerly duct, as indicated in Matthews and Kiladis (1999).

7. Convectively coupled Kelvin waves

It has been shown in sections 4 and 5 that the Kelvin wave wind and associated convection both vary with ENSO phases. The convective coupling of Kelvin waves will be examined in this section. The focus will be on the coupled waves in the central-eastern Pacific region.

a. Horizontal structure

Figure 8 shows composite horizontal structures of convectively coupled Kelvin waves at various levels in the sector 180°–90°W, obtained by regressing the Kelvin wave u and the eastward-moving OLR onto the extrema in the equatorial u at the level considered. Compared with La Niña winters, the convective signals associated with Kelvin waves at all levels are generally stronger and more centered on the equator in El Niño winters, consistent with that indicated in Figs. 2–4. In La Niña winters the convection tends to be centered in the NH off-equatorial region, consistent with the strong NH extratropical forcing there.

Convective coupling of the Kelvin wave is basically consistent with theory, the 850-hPa convergence being in phase or slightly ahead of the intensified convection and 200-hPa divergence in phase with the convection. The Kelvin wave at 100 hPa is also closely coupled with convection. At 70 hPa the convective coupling is still evident in El Niño winters but less clear in La Niña winters, indicating that in El Niño winters there is enhanced propagation into the lower stratosphere of convectively coupled Kelvin waves, consistent with stronger equatorial convection in this case.

An example of a convectively coupled Kelvin wave in summer is shown in Figs. 8e,f. It shows that in summer convectively coupled Kelvin waves over the central-eastern Pacific region are also stronger in El Niño than in La Niña. However, in both ENSO phases, regressed convection is less centered on the equator but shifted to around 8°–10°N where the summer ITCZ is located.

Convectively coupled Kelvin waves in the EH (not shown) are generally stronger than in the WH and show more upward propagation into the lower stratosphere in both ENSO phases. The convective signal associated with the wave at 70 hPa is slightly weaker in El Niño than in La Niña winters. Nevertheless, the difference is smaller than that over the central-eastern Pacific.

b. Zonal propagation

Figure 9 shows the composite zonal propagation of Kelvin waves at both 100 and 850 hPa and the associated convection in El Niño and La Niña winters and summers, obtained by regressing the Kelvin wave equatorial u and eastward-moving OLR averaged latitudinally between 10°N and 10°S onto the extrema in the equatorial u in the 180°–90°W sector. The extrema are taken to be positive and relocated to 0° longitude and day 0. In the winter case (Figs. 9a,b), a few features stand out. First, both the Kelvin wave u and associated convection are stronger in El Niño than in La Niña winters, especially at 100 hPa. Second, in El Niño winters, the Kelvin wave u at 100 hPa and the associated convection indicate a consistent coupling, with the u divergence being ahead of the intensified convection. The remarkable spatial coherency lasts typically for at least one week, whereas in La Niña winters the convective coupling is less

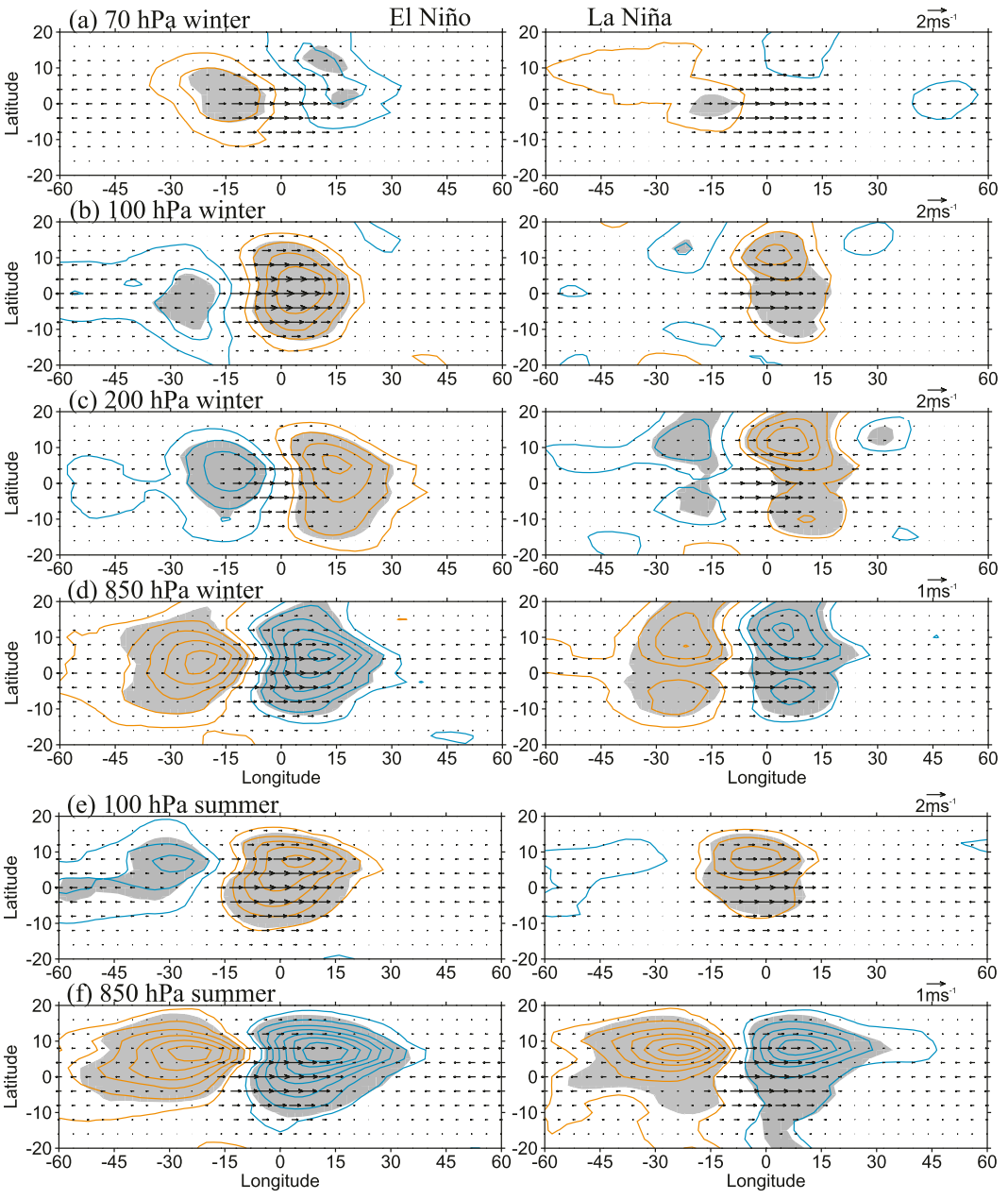

FIG. 8. Horizontal structure of eastward-moving OLR (contours) and the Kevin wave winds (vectors) at various levels for two ENSO phases in (a)–(d) winter and (e),(f) summer, obtained by regressing Kelvin wave u and OLR onto the extrema in the Kelvin wave equatorial u at that level for 180°–90°W. The extreme u is taken to be westerly and located at 0° relative longitude, with a value of 1.5 times its peak SD. The blue (red) contours are for negative (positive) OLR, contour interval 1 W m^{-2}; the zero contour is not drawn. The shaded areas denote OLR regions that exceed the 95% significance level.

coherent. The lower-level convective coupling is also very coherent and lasts longer in El Niño winters. Third, coupled Kelvin waves at 100 hPa have a faster phase speed (14 m s^{-1}) in El Niño than in La Niña winters (11 m s^{-1}), in agreement with Fig. 2 where the WH power spectral signal appears at larger equivalent depths in El Niño than in La Niña winters.

It is also clear that for both ENSO phases the low-level coupled wave has a faster phase speed (17 m s^{-1}), smaller k (3–4), and a shorter period (7 days) than those at 100 hPa (c = 11–14 m s^{-1}, k = 5, and period 8 days). The generally faster phase speeds of the low-level Kelvin waves are also found in other regions. The reason for this difference is not clear.

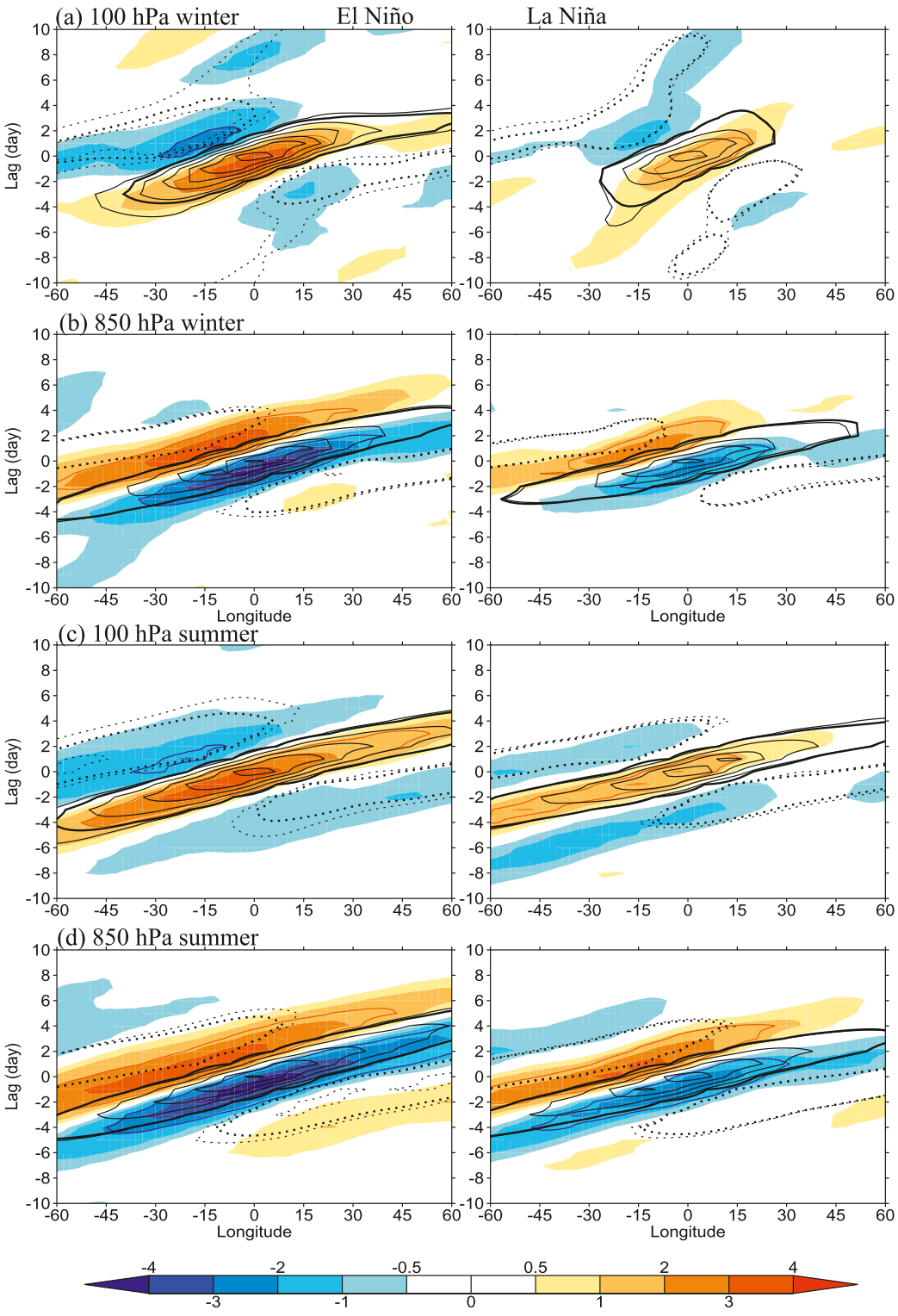

FIG. 9. Longitude–time diagram of eastward-moving OLR (color, W m^{-2}) and Kelvin wave equatorial u (black thin contours) at 100 and 850 hPa, regressed onto the extrema in the Kelvin wave equatorial u for 180°–90°W for El Niño and La Niña in (a),(b) winter, and (c),(d) summer. The extreme u is taken to be westerly and located at 0° relative longitude at day 0, with a value of 1.5 times its peak SD. The contour interval for winds is 0.4 m s^{-1} at 100 hPa and 0.2 m s^{-1} at 850 hPa with negative winds dotted and zero contour not drawn. Thick black (color) contours show areas of winds (OLR) that exceed the 95% significance level.

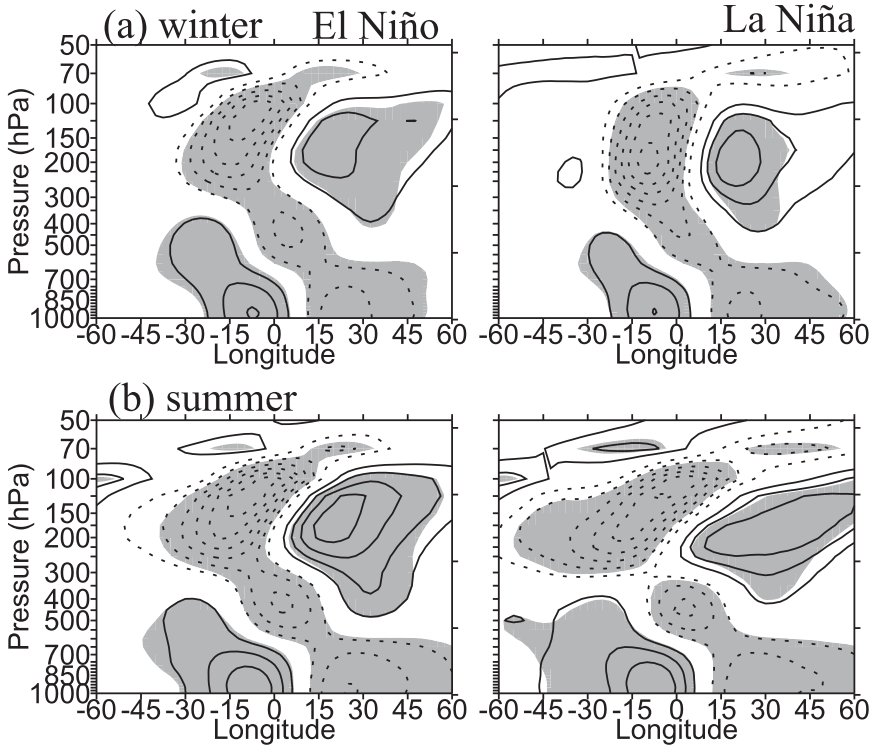

FIG. 10. Vertical structure of Kelvin wave equatorial u in El Niño and La Niña winters and summers, regressed onto the extrema of eastward-moving OLR at 10°N–10°S over the sector 180°–90°W. The extreme OLR is located at 0° relative longitude with a negative value of 1.5 times its peak SD. Positive (solid contour) and negative (dotted contour) winds are shown with a contour interval of 0.3 m s^{-1}, and zero contours are not drawn. The shaded areas denote regions of regressed values exceeding the 95% significance level.

As in the winter case, convectively coupled Kelvin waves in summer are stronger in El Niño than in La Niña (Figs. 9c,d). However, in contrast to the winter case, coupled waves in summer have very similar phase speeds in the upper and lower troposphere for both ENSO phases, suggesting that the coupled waves have stronger vertical coupling in summer than in winter. In La Niña summers the convective signal connected to the waves at both levels is clearly biased to negative temporal lag; that is, the convection leads the Kelvin wave wind. This suggests that in this case the convection forces the Kelvin wave.

The coupled waves in the EH region (not shown) indicate different coupling features at the lower level, with the intensified convection being in phase with the convergence in the early stages and then almost in phase with equatorial westerly wind in later stages. This lower-level coupling feature in the EH was also shown in YHS and YHS07a,c.

c. *Vertical structure*

To show the vertical structure of convectively coupled Kelvin waves, the Kelvin wave equatorial u at each level is regressed onto the extrema in the eastward-moving OLR averaged within 10°N–10°S. The OLR extrema are relocated to 0° relative longitude and the sign is taken to be negative to represent intensified convection. Looking at the upper- and lower-tropospheric structures only, the vertical structure looks like a first internal mode, with the lower-level convergence being slightly ahead of the intensified convection, but the 200-hPa divergence being in phase with the convection. The vertical tilt, with the upper-level Kelvin wave shifting to the west of the lower-level wave as compared with the first internal vertical mode, is more obvious in the summer case (Fig. 10b). This feature is also seen in other observational studies (e.g., Straub and Kiladis 2003; YHS07a).

However, the Kelvin wave is not that of a simple first internal mode as might be speculated from the upper- and lower-level structures only. In addition to the two peaks in the upper and lower troposphere, the Kelvin wave has another peak in the middle troposphere around 500 hPa that is stronger in summer, so the vertical structure could be viewed as a mixture of the first and second internal modes. This feature was also found in YHS07a.

In all cases, except for the La Niña winters, the waves above 200 hPa have an eastward tilt with height and the wave signal extends upward into the lower stratosphere. This is an indication of coupled Kelvin waves propagating into the lower stratosphere. The eastward tilt with height in the upper troposphere and lower stratosphere is consistent with that found by Wheeler et al. (2000), YHS07a, YHS11, and YHG12.

For the exception of La Niña winters, the peak in the upper troposphere is located at a lower level around 200 hPa, in contrast to the other cases where it is above 125–150 hPa. This is consistent with the local maximum of the wave amplitude there (Fig. 5f) and the associated extratropical forcing (Fig. 6b). Although the Kelvin wave amplitude around 200 hPa seems to be stronger in La Niña winters owing to the stronger extratropical forcing, there is less convectively coupled wave signal propagating upward into the lower stratosphere. This is consistent with the wave having less vertical coupling, as mentioned in the last section.

8. Summary and discussion

In this paper, the impact of ENSO on the behavior of equatorial Kelvin waves and their associated convection has been examined using ERA-Interim data and the YHS methodology in identifying equatorial waves. The major results found here will be summarized.

The phase of ENSO has a significant impact on Kelvin waves and their associated convection over the equatorial central-eastern Pacific. El Niño (La Niña) events enhance (suppress) the variability of eastward-moving Kelvin wave–related convection and the Kelvin wave wind itself, especially in the upper troposphere and lower stratosphere, both in winter and summer.

The impact of the ENSO on Kelvin waves is through changes in the ENSO-related thermal conditions and ambient zonal flows. First, in El Niño years, because convection intensifies in response to the warming of the underlying SSTs in the equatorial central-eastern Pacific, the variability of tropical eastward-moving convection, which is mainly associated with Kelvin waves, also intensifies in this region. Second, owing to the equatorial main convective region moving eastward in El Niño years, the equatorial eastern Pacific westerly duct in the upper troposphere is significantly reduced in El Niño winters or disappears in El Niño summers, leading to an amplification of the in situ upper-tropospheric Kelvin waves. These two factors lead to Kelvin waves being more convectively and vertically coupled in El Niño years, and there is enhanced convectively coupled Kelvin wave propagation upward into the lower stratosphere over the central-eastern Pacific region. In La Niña years the opposite occurs.

However, it is found that in winter the ENSO-related change in zonal flow also has a clear impact on modulating the propagation of NH extratropical Rossby waves into the equatorial region, which affects the behavior and intensity of Kelvin waves there. The strongest impact occurs in La Niña winters when the stronger eastern Pacific westerly duct allows more NH extratropical eastward-moving Rossby waves propagation into the equatorial region in the upper troposphere and force Kelvin waves around 200 hPa, leading to a local Kelvin wave peak there. This partly offsets the in situ weakening effect of the stronger ambient westerly on Kelvin waves. It is also found that the extratropical forcing leads to eastward-moving equatorial R1 waves that interfere with the Kelvin wave in the upper troposphere, leading to strong geopotential heights but weak zonal wind fields in the equatorial region. Because of the suppressed equatorial convection in the region in La Niña years the forced Kelvin wave is less vertically and convectively coupled, and there are fewer waves reaching 100 hPa and then upward propagating into the lower stratosphere.

In other tropical regions, the ENSO impact on Kelvin waves and their associated convection is generally not so clear. However, in winter over the equatorial eastern Indian–western Pacific Oceans. Kelvin waves in the upper troposphere and their associated convection are slightly weaker in El Niño than in La Niña. Nevertheless, the difference is much smaller than that over the central-eastern Pacific.

ENSO-related differences are predominantly over the central-eastern Pacific, but for tropical averages the Kelvin waves in the upper troposphere and lower stratosphere and their associated convection are still stronger in El Niño than in La Niña years. This is consistent with a modeling study of Maury et al. (2013), which shows that in El Niño years there are stronger Kelvin waves in the lower stratosphere.

That an El Niño event enhances the Kelvin wave–related convection and wind itself and a La Niña event suppresses them has not been revealed in previous observational studies. The impact of ENSO on propagation of convectively coupled Kelvin waves into the lower stratosphere is also a new finding. As the Kelvin wave is the main forcing of the QBO westerly winds, the results found in this study provide a potential link between the ENSO and QBO. Maruyama and Tsuneoka (1988) noted that the rapid descent of QBO westerlies often occurred with El Niño events. This may be explained by the results obtained here that El Niño events enhance the Kelvin wave activity in the lower stratosphere, which is the driver of the rapid descent of the QBO westerly phase. However, some studies suggest that the stratospheric QBO influences the ENSO variability (e.g., Gray

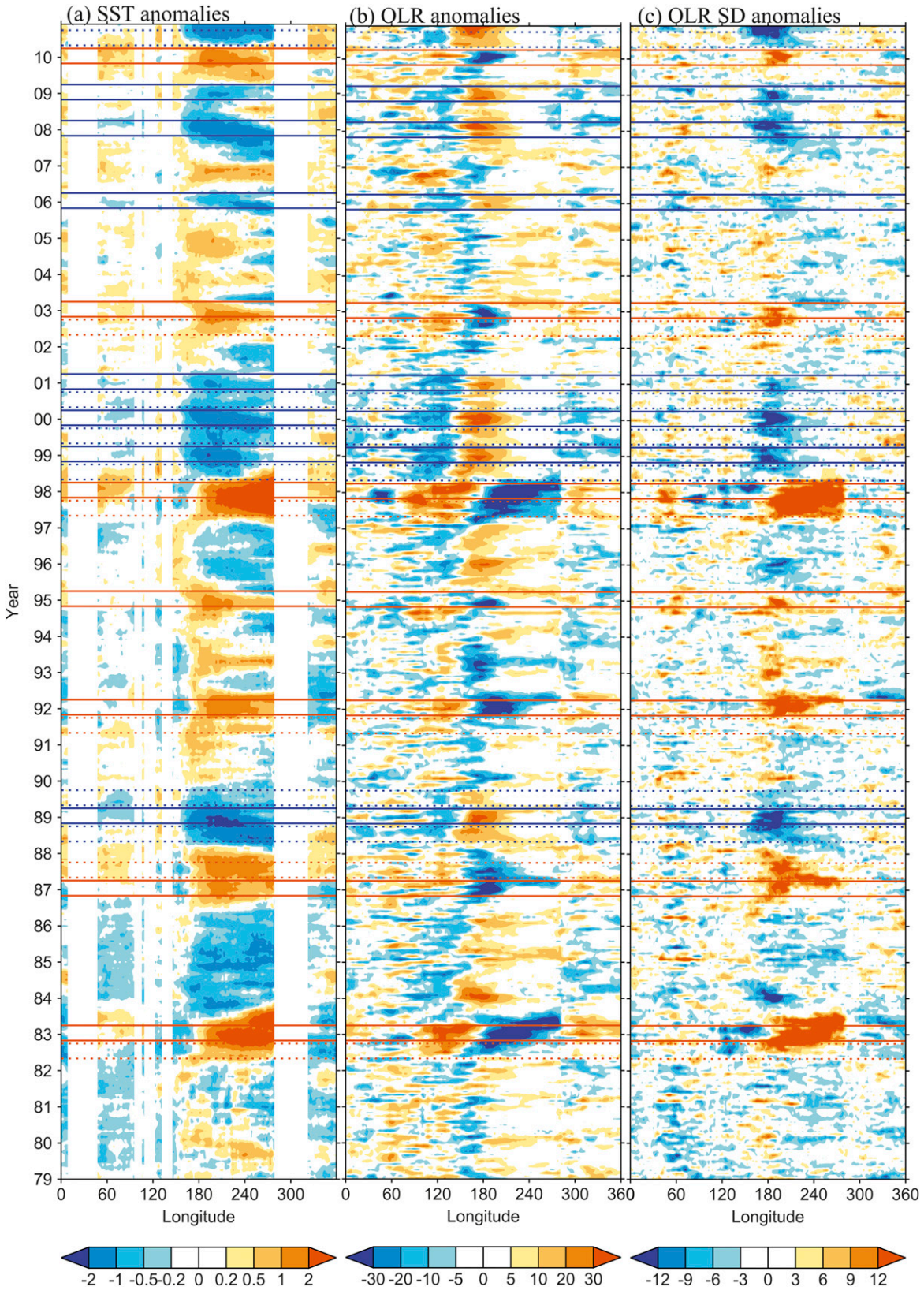

FIG. A1. Hovmöller plots of monthly equatorial (5°N–5°S) anomalies of (a) SST, (b) OLR, and (c) SD of OLR (departure from monthly mean) from 1979 to 2010. Each pair of solid red (blue) lines indicate El Niño (La Niña) winters, and each pair of dotted red (blue) lines indicated El Niño (La Niña) summers.

et al. 1992), and other studies suggest no relationship between QBO and ENSO (e.g., Kane 2004). Nevertheless, it is believed that the results revealed in this study are important not only for weather forecasting in the troposphere but also for stratospheric behavior.

It is recognized that the sample size for compositing is not large. However, analysis for individual events, as shown by Fig. 4, indicates that the difference between the two ENSO phases is found for almost all individual El Niño/La Niña events. This is supportive of the significance of the results despite the small sample size. If less strict thresholds are used (e.g., Niño-3.4 index only), there will be three more La Niña winters (1983/84, 1984/85, and 1995/96), three more La Niña summers (1984, 1985, and 2007), but only one more El Niño summer (2009). Composites including these extra El Niño/La Niña events also indicate similar results, but with the difference between the ENSO phases being slightly reduced. Also, it is noteworthy that most La Niña winters occur after 1998. This may be associated with decadal changes in ENSO. Sun and Yu (2009) showed that there is, indeed, a 10–15-yr cycle in ENSO intensity. In their study, 1988–96 was the weakening stage of the ENSO cycle, consistent with only one La Niña being identified in this period.

This study has focused only on the ENSO impact on the Kelvin wave, but it is of interest to investigate the ENSO impact on other equatorial waves. This will be the subject of a subsequent paper. Since the last decade, a number of studies have shown that different types of ENSO are related to the location of the center of SST anomalies (e.g., Larkin and Harrison 2005; Ashok et al. 2007). An investigation of their differing impact on the equatorial waves and tropical convection would also be of interest.

Acknowledgments. We thank the two anonymous reviewers for their very helpful comments. GYY acknowledges the support of the National Centre for Atmospheric Science (NCAS). GYY is a member of NCAS.

APPENDIX

Evolution of Monthly Equatorial SST and Convection

To give a picture of ENSO evolution and its relationship with equatorial convective activity, Fig. A1 shows monthly anomalies of equatorial SST, OLR, and its standard deviation (daily data departure from monthly mean). The ENSO evolution is clearly seen in the equatorial SSTA, with strong warm events occurring in 1982/83 and 1997/98 and weaker warm events in 1991/92, 1986/87, 1994/95, 2002/03, and 2009/10. It is seen that SSTAs are generally stronger in winter than in summer. For some prolonged events (lasting a few seasons), El Niño tends to be initiated in summer and continue through the following winter, except for the 1986/87 event. After the 1982/83 strong warm phase, there is a prolonged cold phase from the middle of 1983 to 1986; however, since the Southern Oscillation index in these period is weak, no La Niña events are defined here, as seen in Fig. 1. Following the strongest warm phase in 1997/98, there is also a prolonged 3-yr cold phase with several La Niña seasons being defined, starting immediately after summer 1998.

It is seen that, as for the SST signal, the convective signal is also generally stronger in winter than in summer. In El Niño years the convective region that is normally over Indonesia and the far western Pacific moves eastward into the central Pacific, with negative OLR anomalies appearing over a distance of several thousand miles along the equator over the central-eastern Pacific but positive anomalies over Indonesia to the western Pacific. In La Niña years the situation is reversed but with positive OLR anomalies occurring in a narrower longitudinal range over the central Pacific. Over the central-eastern Pacific, negative (positive) OLR anomalies that correspond to heating (cooling) are coincident with a warm (cold) SSTA, indicating that during El Niño (La Niña) years convection is intensified (suppressed) in response to the warming (cooling) of the underlying SST.

Monthly OLR standard deviation (SD) anomalies are only strong over the central-eastern Pacific with positive SD anomalies in El Niño coincident with regions of negative OLR anomalies and warm SST there, and vice versa for negative SD anomalies in La Niña. Over the western Pacific, ENSO-related SD anomalies are weaker except for the 1982/83 and 1997/98 strong El Niño events, where there are strong negative anomalies. This indicates that over the central-eastern Pacific, ENSO-related convective variability has time scales shorter than one month, whereas over the western Pacific the ENSO-related variability on such time scales is not significant except for strong El Niño events when equatorial convection is very weak. It is suggestive that ENSO-related convection variability in the western Pacific region is dominated by longer time scales.

REFERENCES

Ashok, K., S. K. Behera, S. A. Rao, H. Weng, and T. Yamagata, 2007: El Niño Modoki and its possible teleconnection. *J. Geophys. Res.,* **112,** C11007, doi:10.1029/2006JC003798.

Barnston, A. G., and R. E. Livezey, 1987: Classification, seasonality and persistence of low-frequency atmospheric circulation patterns. *Mon. Wea. Rev.,* **115,** 1083–1126.

Bretherton, F. P., and C. J. R. Garrett, 1968: Wave trains in inhomogeneous moving media. *Proc. Soc. London,* **362A,** 529–554.

Chou, C., J.-Y. Tu, and J.-Y. Yu, 2003: Interannual variability of the western North Pacific summer monsoon: Differences

between ENSO and non-ENSO years. *J. Climate,* **16,** 2275–2287.

Dee, D. P., and Coauthors, 2011: The ERA-Interim reanalysis: Configuration and performance of the data assimilation system. *Quart. J. Roy. Meteor. Soc.,* **137,** 553–597.

Gill, A. E., 1980: Some simple solutions for heat-induced tropical circulations. *Quart. J. Roy. Meteor. Soc.,* **106,** 447–462.

Gray, W. M., J. D. Sheaffer, and J. A. Knaff, 1992: Hypothesized mechanism for stratospheric QBO influence on ENSO variability. *Geophys. Res. Lett.,* **19,** 107–110.

Hoskins, B. J., and G.-Y. Yang, 2000: The equatorial response to higher-latitude forcing. *J. Atmos. Sci.,* **57,** 1197–1213.

Kane, R. P., 2004: Comparison of stratospheric zonal winds and El Niño–Southern Oscillation in recent decades. *Int. J. Climatol.,* **24,** 525–532, doi:10.1002/joc.1004.

Kawamura, R., T. Matsuura, and S. Iizuka, 2001: Interannual atmosphere-ocean variations in the tropical western North Pacific relevant to the Asian summer monsoon-ENSO coupling. *J. Meteor. Soc. Japan,* **79,** 883–898.

Kiladis, G. N., 1998: Observations of Rossby waves linked to convection over the eastern tropical Pacific. *J. Atmos. Sci.,* **55,** 321–339.

Kushnir, Y., and J. M. Wallace, 1989: Low-frequency variability in the Northern Hemisphere winter: Geographical distribution, structure and time-scale dependence. *J. Atmos. Sci.,* **46,** 3122–3143.

Larkin, N. K., and D. E. Harrison, 2005: Global seasonal temperature and precipitation anomalies during El Niño autumn and winter. *Geophys. Res. Lett.,* **32,** L16705, doi:10.1029/2005GL022860.

Lau, K.-M., and L. Peng, 1987: Origin of low-frequency (intraseasonal) oscillations in the tropical atmosphere. Part I: Basic theory. *J. Atmos. Sci.,* **44,** 950–972.

Liebmann, B., and C. A. Smith, 1996: Description of a complete (interpolated) outgoing longwave radiation dataset. *Bull. Amer. Meteor. Soc.,* **77,** 1275–1277.

Lim, H., and C.-P. Chang, 1983: Dynamics of teleconnections and Walker circulations forced by equatorial heating. *J. Atmos. Sci.,* **40,** 1897–1915.

Lin, J.-L., and Coauthors, 2006: Tropical intraseasonal variability in 14 IPCC AR4 climate models. Part I: Convective signals. *J. Climate,* **19,** 2665–2690.

Lindzen, R. S., and J. R. Holton, 1968: A theory of the quasi-biennial oscillation. *J. Atmos. Sci.,* **25,** 1095–1107.

Maruyama, T., and Y. Tsuneoka, 1988: Anomalously short duration of the easterly wind phase of the QBO at 50 hPa in 1987 and its relationship to an El Niño event. *J. Meteor. Soc. Japan,* **66,** 629–634.

Matthews, A. J., and G. N. Kiladis, 1999: Interactions between ENSO, transient circulation, and tropical convection over the Pacific. *J. Climate,* **12,** 3062–3086.

Maury, P., F. Lott, L. Guez, and J.-P. Duvel, 2013: Tropical variability and stratospheric equatorial waves in the IPSLCM5 model. *Climate Dyn.,* **40,** 2331–2344, doi:10.1007/s00382-011-1273-0.

Rasmusson, E. M., and T. H. Carpenter, 1982: Variations in tropical sea surface temperature and surface wind fields associated with the Southern Oscillation/El Niño. *Mon. Wea. Rev.,* **110,** 354–384.

Redelsperger, J.-L., and Coauthors, 1998: Review of convection in TOGA-COARE. *Proc. CLIVAR/GEWEX COARE98 Conf.,* Boulder, CO, WCRP, 16–42.

Ringer, M. A., and Coauthors, 2006: The physical properties of the atmosphere in the new Hadley Centre Global Environmental Model (HadGEM1). Part II: Aspects of variability and regional climate. *J. Climate,* **19,** 1302–1326.

Sakai, K., and R. Kawamura, 2009: Remote response of the East Asian winter monsoon to tropical forcing related to El Niño–Southern Oscillation. *J. Geophys. Res.,* **114,** D06105, doi:10.1029/2008JD010824.

Salby, M. L., H. H. Hendon, K. Woodberry, and K. Tanaka, 1991: Analysis of global cloud imagery from multiple satellites. *Bull. Amer. Meteor. Soc.,* **72,** 467–480.

Slingo, J. M., K. R. Sperber, J.-J. Morcrette, and G. L. Potter, 1992: Analysis of the temporal behavior of convection in the tropics of the European Centre for Medium-Range Weather Forecasts model. *J. Geophys. Res.,* **97** (D16), 18 119–18 135.

Straub, K. H., and G. N. Kiladis, 2003: The observed structure of convectively coupled Kelvin waves: Comparison with simple models of coupled wave instability. *J. Atmos. Sci.,* **60,** 1655–1668.

Sun, F., and J.-Y. Yu, 2009: A 10–15-yr modulation cycle of ENSO intensity. *J. Climate,* **22,** 1718–1735.

Trenberth, K. E., J. M. Caron, D. P. Stepaniak, and S. Worley, 2002: Evolution of El Niño–Southern Oscillation and global atmospheric surface temperatures. *J. Geophys. Res.,* **107,** 4065, doi:10.1029/2000JD000298.

Troup, A. J., 1965: The 'Southern Oscillation.' *Quart. J. Roy. Meteor. Soc.,* **91,** 490–506.

Wallace, J. M., and D. S. Gutzler, 1981: Teleconnections in the geopotential height field during the Northern Hemisphere winter. *Mon. Wea. Rev.,* **109,** 784–812.

Wang, B., and X. Xie, 1996: Low-frequency equatorial waves in vertically sheared zonal flow. Part I: Stable waves. *J. Atmos. Sci.,* **53,** 449–467.

——, R. Wu, and X. Fu, 2000: Pacific–East Asian teleconnection: How does ENSO affect East Asian climate? *J. Climate,* **13,** 1517–1536.

Weare, B. C., 2006: Centered composite analysis of variations associated with the Madden–Julian oscillation. *J. Climate,* **19,** 1834–1849.

Wheeler, M., and G. N. Kiladis, 1999: Convectively coupled equatorial waves: Analysis of clouds and temperature in the wavenumber–frequency domain. *J. Atmos. Sci.,* **56,** 374–399.

——, ——, and P. J. Webster, 2000: Large-scale dynamical fields associated with convectively coupled equatorial waves. *J. Atmos. Sci.,* **57,** 613–640.

Yang, G.-Y., and B. J. Hoskins, 1996: Propagation of Rossby wave of nonzero frequency. *J. Atmos. Sci.,* **53,** 2365–2378.

——, ——, and J. M. Slingo, 2003: Convectively coupled equatorial waves: A new methodology for identifying wave structures in observational data. *J. Atmos. Sci.,* **60,** 1637–1654.

——, ——, and ——, 2007a: Convectively coupled equatorial waves: Part I: Horizontal structure. *J. Atmos. Sci.,* **64,** 3406–3423.

——, ——, and ——, 2007b: Convectively coupled equatorial waves: Part II: Zonal propagation. *J. Atmos. Sci.,* **64,** 3424–3437.

——, ——, and ——, 2007c: Convectively coupled equatorial waves: Part III: Synthesis structures and extratropical forcing. *J. Atmos. Sci.,* **64,** 3438–3451.

——, J. M. Slingo, and B. J. Hoskins, 2009: Convectively coupled equatorial waves in high-resolution Hadley Centre climate models. *J. Climate,* **22,** 1897–1919.

——, B. J. Hoskins, and J. M. Slingo, 2011: Equatorial waves in opposite QBO phases. *J. Atmos. Sci.,* **68,** 839–862.

——, ——, and L. Gray, 2012: The influence of the QBO on the propagation of equatorial waves into the stratosphere. *J. Atmos. Sci.,* **69,** 2959–2982.

Zhang, R., A. Sumi, and M. Kimoto, 1996: Impact of El Niño on the East Asian monsoon: A diagnostic study of the '86/87 and '91/92 events. *J. Meteor. Soc. Japan,* **74,** 49–62.